HOSTED BY
ELSEVIER
Available online at www.sciencedirect.com
ScienceDirect
Soils and Foundations 63 (2023) 101328
www.elsevier.com/locate/sandf

Technical Paper

On the modelling of stress-dilatancy behavior in weakly cemented sands

Saurabh Singh [a], Ramesh Kannan Kandasami [b], Tejas G. Murthy [a,*], Matthew Richard Coop [c]

[a] *Indian Institute of Science, Bangalore 560012, India*
[b] *Indian Institute of Technology Madras, Chennai 600036, India*
[c] *University College London, London WC1E6BT, United Kingdom*

Received 5 October 2022; received in revised form 5 April 2023; accepted 23 May 2023

Abstract

A comprehensive study on the stress-dilatancy behavior of cemented sand and its modeling is presented. The effect of confining pressure, relative density, and cement content on stress-dilatancy behavior are studied from the published experimental results and an additional series of experiments performed in this study. To facilitate a contrast and comparison of stress-dilatancy behavior between these datasets, a normalized stress ratio is proposed which removes the effect of mineralogy and morphology of parent sand. A set of key insights were obtained from this comparative study which aided in improving the stress-dilatancy relation; for example, the effect of initial conditions on stress-dilatancy behavior was found to be captured by the ratio of cohesion intercept (or tensile strength) and mean effective stress before shearing. The limitations of stress transformation, often used in modelling of cemented sand, were also systematically studied by a set of carefully designed experiments; it was found to be only applicable before gross yielding of cementation. After gross yielding, it is necessary to take in account of the breakage of bonds/cementation. The gross yield locus was identified from 70 experimental datasets and a cohesion/bond degradation model was formulated to model the stress-dilatancy behavior of cemented sand. The efficacy of stress-dilatancy relations (after including the gross yield locus and bond degradation behavior) is evaluated from the experimental results; the Rowe's stress-dilatancy relation was found to be most suitable with the proposed bond/cohesion degradation model.

Keywords: Stress transformation; Stress-dilatancy; Interparticle cohesion; Bond degradation

1. Introduction

Geomaterials such as cemented sand, structured soils, and soft sandstones are often encountered in the infrastructure, offshore, mining and petroleum sectors. While such geomaterials are ubiquitous in the field, soil constitutive models of various degrees of complexity have predominantly focused on clean sand and soft clays. In order to predict the mechanical behavior of geomaterials such as cemented sands, which neither belong to the class of soils or rocks, constitutive models developed for sand are suitably modified by introducing the inter-particle cohesion/bond strength to account for cementation. Kim and Lade (1984); Houlsby (1986); Reddy and Saxena (1992); Matsuoka and Sun (1995); Yao et al. (2004) have extended constitutive models or failure criterion of sand to cemented sand by accounting for the cohesion/cementation (as an additional confinement).

As is the case with sand, experimental studies on cemented sand have also revealed that the response is governed by mean effective stress p', void ratio e, and intermediate principal stress ratio b (Reddy and Saxena, 1992; Cuccovillo and Coop, 1999; Abdulla and Kiousis, 1997; Bachus et al., 1981; Schnaid et al., 2001; Kandasami et al., 2021). In addition, type and amount of cementation

* Corresponding author.
E-mail address: tejas@iisc.ac.in (T.G. Murthy).

https://doi.org/10.1016/j.sandf.2023.101328
0038-0806/

Nomenclature

α	Nova-Wood stress dilatancy parameter
b	intermediate stress ratio
c	cohesion intercept
c_0	initial cohesion intercept
CC	cement content
D	dilatancy
D_{50}	mean grain size
D_{max}	maximum dilatancy
D_p	plastic dilatancy
D_r	relative density
e	void ratio
e_{max}	maximum void ratio
e_{min}	minimum void ratio
ε_v	volumetric strain
ε_q	deviatoric shear strain $\sqrt{\frac{4}{3}J_{2\epsilon}}$ or $\frac{2}{3}(\epsilon_1 - \epsilon_3)$
ε_v^p	plastic volumetric strain
ε_q^p	plastic deviatoric shear strain
J_{2T}	second invariant of deviatoric part of tensor T
η	stress ratio
η_p	peak stress ratio
η_{yield}	stress ratio for gross yield
φ	friction angle
G	shear modulus
K	bulk modulus
M	critical state stress ratio
$\frac{M-\eta}{\alpha}$	normalized stress ratio
ν	Poisson's ratio
p'	mean effective stress
p'_i	initial mean effective stress
q	deviatoric shear stress $\sqrt{3J_{2\sigma}}$ or $(\sigma_1 - \sigma_3)$

also contributes to the mechanical response of cemented sand (Schnaid et al., 2001; Ismail et al., 2002; Consoli et al., 2007). There are very many constitutive models that carefully parse the various behavioral facets of cemented sands (Yu et al., 2007; Tengattini et al., 2014; Rahimi et al., 2016; Gao and Zhao, 2012), however most of these constitutive models require significant experimental effort to arrive at the model parameters and the overall implementation is computationally expensive.

The stress-dilatancy relations plays a crucial role in constitutive modeling of sand; it forms a basis for evolution of plastic strains. These relations are often modified to accommodate the effect of cementation for modelling the behavior of cemented sand. The cementitious bonds restrain the movement of sand particles which leads to an increase in the normal and tangential stiffness at the contact. This presence of cementation is akin to presence of an additional confinement to an equivalent sand element -- the effect of cementation is modelled by using a coordinate transformation in stress space i.e., state boundary surfaces (used in modelling of sand) are translated along the hydrostatic axis by a distance of "bond or tensile strength. To determine bond strength for this coordinate transform (stress transformation), laboratory techniques such as Brazilian tests (Das et al., 1995), triaxial extension tests (Airey, 1993), and uniaxial extension tests (Lade, 1982) have been used. The bond strength of cemented sand is also estimated from intercept of Mohr-Coulomb peak state envelope on the σ-axis (Gao and Zhao, 2012). This approach of stress transformation is simplistic and does not capture the complex response of cemented sands; while this has been recognized, a careful examination of the limitations and disadvantages of such a stress transformation approximation has been missing. In this paper, a study has been made through a series of experiments, wherein the adequacy and limitation of stress transformation is critically examined.

Among the stress dilatancy relationships available for cemented sands, Rowe, 1962; Zhang and Salgado, 2010 are all simple extensions of or identical to stress dilatancy relations of sand. In this article, a large dataset (a series of triaxial experiments conducted in this testing program and triaxial tests digitized from literature) - is used to assess the efficacy of these stress-dilatancy relations and to highlight various aspect of stress-dilatancy behavior of cemented sand. A new normalized stress ratio is proposed to facilitate the comparison of stress dilatancy behavior of cemented sand with different parent sand (for digitized experiments). Additionally, cohesion degradation, which is well documented in experiments, has been incorporated into the stress-dilatancy relations after the gross yielding of bonds. This incorporation of cohesion degradation significantly improves the quality of predictions.

2. Experiments and theory

2.1. Experiments

In this experimental programme, three suites of monotonic drained triaxial compression tests are performed to examine the efficacy of utilizing an equivalent confining pressure (stress transformation) to replicate inter-particle cohesion and to examine the stress-dilatancy response of cemented sand.

2.2. Materials

Quartzitic angular sand (with particle sphericity = 0.42 and roundness = 0.17, specific gravity = 2.65, mean grain size D_{50} = 0.45 mm, e_{max} = 0.97 and e_{min} = 0.54) was used

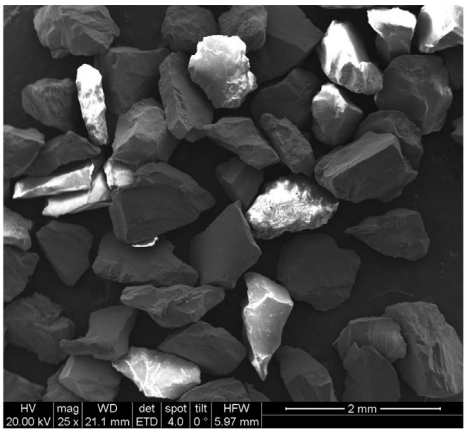

(a) A micrograph of sand particles

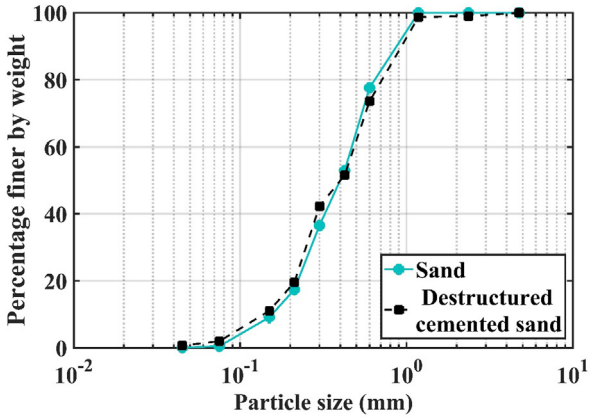

(b) Grain size distribution of sand and cemented sand-post failure

Fig. 1. Morphological characteristics of sand and cemented sand.

along with ordinary Portland cement (OPC-53 grade, specific gravity = 3.15) as a binder material (4% by weight of sand) for preparing the cemented sand specimens (cured in moist environment for 14 days) in this experimental program (Fig. 1). All the sand and cemented sand specimens (diameter – 100 mm, height – 200 mm) were prepared to the same unit weight of 15 kN/m^3 (relative density D_r – 46.5%) prior to testing. All the specimens were saturated at an effective stress of 20 kPa followed by isotropically consolidating it to a desired effective mean stress and shearing at a displacement rate of 0.1 mm/min.

2.3. Test matrix

In series #1 (cemented sand), weakly cemented sand specimen, prepared in the laboratory, were consolidated to a mean effective stress of 50, 150, 300, 450 kPa before shearing. In series #2 (control sand), triaxial compression tests were performed on water-pluviated clean sand specimens consolidated to same mean effective stresses as in series #1. In series #3 (equivalent sand), using the hypothesis that cementation can be treated as an additional confinement on the specimen, tests on clean sand were performed at an "equivalent confining pressure".

The bond strength for cemented sand was estimated to be 114 kPa from intercept of peak state envelope on p'-axis in the triaxial stress space (p'-q) (Appendix A). Using this value, an "equivalent confining pressure", which accounts for the cohesion, i.e., 164, 264, 414 and 564 kPa (50 + 114 = 164; 150 + 114 = 264; 300 + 114 = 414 and 450 + 114 = 564) was utilized in series #3.

A direct comparison of cemented sand and clean sand (without adding the fines in sand) was possible for 4% cement content, because such small content of fines does not change the sand behavior of significantly (Rad and Clough, 1982).

3. Stress transformation for weakly cemented sand

In this section, stress transformation is studied – the state of a cemented granular material subjected to a uniform stress state is identical to the state of the frictional granular material subjected to same boundary conditions and additional confining pressure equivalent to the bond strength of cemented granular material (Caquot, 1934) – to carefully establish its limitations and advantages.

Fig. 2 shows the stress–strain and volumetric response (contraction is positive), respectively for the experiments carried out on the control clean sand, equivalent sand, and cemented sand. At low strain levels (up to 1–2.5%), the behavior of the cemented sand and of the corresponding equivalent sand is almost identical (Fig. 2a and Fig. 2b), however, at larger strains the deviation in response increases. Cemented sand specimens reach a peak in the deviatoric stress much earlier (i.e., at much lower strains) than the equivalent sand. Further, the peak strength of cemented sand is much lower than corresponding equivalent sand. At low confining pressures, the post peak response i.e., rate of softening of cemented sand is higher than the equivalent sand. However, this increased softening in cemented sand is suppressed at higher confining pressures. The volumetric strain responses between the cemented sand and the equivalent sand are similar through the entire strain range (Fig. 2c and Fig. 2d).

Fig. 2 suggests that stress-transformation is effective at low strains since the stiffness of cemented sand and equivalent sand are similar. The reason behind this similarity lies in the fact that, at low strain ranges, the inter-particle cementation imparts an additional stiffness to the ensemble which is akin to the effect of increase in confining pressure. At slightly larger strains, this inter-particle cementation begins to break down causing a deviation in the response of cemented sand and equivalent sand. The breakage of bond events can be identified by drastic change in the linear stress–strain response (Coop and Atkinson, 1993; Cuccovillo and Coop, 1997, 1999; Coop and Willson, 2003); in Fig. 2, this can also be seen as a diversion of cemented sand from equivalent sand response.

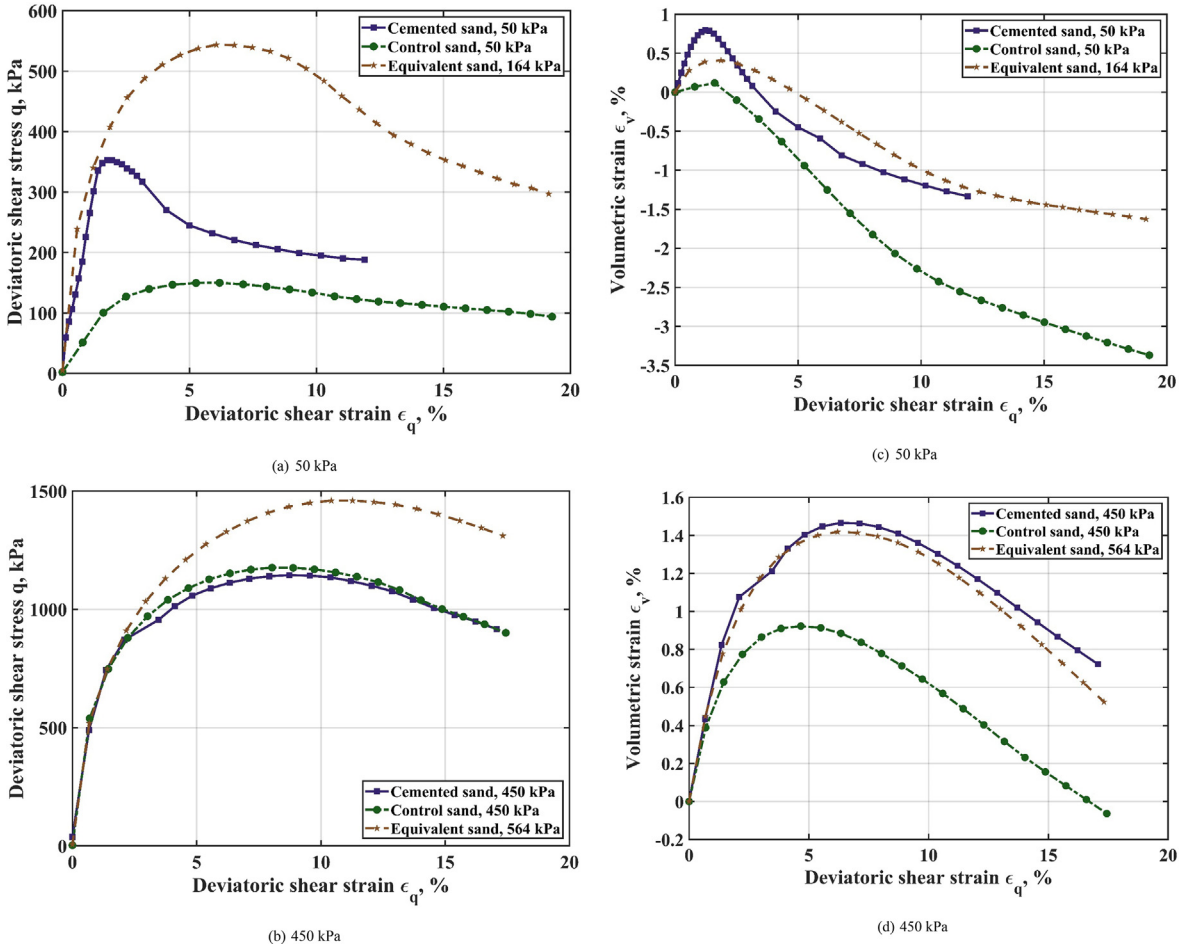

Fig. 2. Stress transformation for cemented sand (a) Stress–strain behavior of cemented sand, control sand, and equivalent sand (b) Volumetric strain vs shear strain behavior of cemented sand, control sand, and equivalent sand.

Table 1
Comparison of observed response between sand and cemented sand.

Effective confining pressure (kPa)	Specimen	Initial stiffness (kPa)	ε_q at q_{peak} (%)	q_{peak} (kPa)	D_{min}	η_p	q_{final} (kPa)
50	Cemented sand	2.47E04	1.86	353	−0.34	1.97	192
	Control sand	6.19E03	5.56	151	−0.24	1.24	57
	Eqvt. sand	3.12E04	6.17	544	−0.15	1.49	180
150	Cemented sand	3.69E04	4.34	483	−0.20	1.51	239
	Eqvt. sand	3.85E04	6.18	755	−0.22	1.44	631
300	Cemented sand	5.21E04	8.82	946	−0.07	1.44	588
	Control sand	3.51E04	8.55	775	−0.09	1.33	589
	Eqvt. sand	5.86E04	9.28	1083	−0.09	1.35	661
450	Cemented sand	6.40E04	9.05	1146	−0.09	1.34	895
	Control sand	6.40E04	8.62	1179	−0.08	1.38	778
	Eqvt. sand	6.33E04	10.75	1463	−0.13	1.36	632

Table 1 presents the comparison of the drained shear response of cemented sand, corresponding equivalent sand, and control sand experiments. The initial stiffness of cemented sand is comparable to equivalent sand at low confining pressure. Peak strength of cemented sand occurs much sooner and is significantly lesser than equivalent sand at low confining pressure whereas at higher confining pressure peak strength of cemented sand and control sand appears to collapse. Cemented sand specimens are more dilative when compared to control or equivalent sand at low confining pressure. The peak stress ratio of cemented sand is much higher than control and equivalent sand at

low confining pressure. At higher confining pressure, the peak stress ratio for cemented sand converges to control sand.

4. Stress-dilatancy in cemented sand

A detailed discussion on stress-dilatancy behavior of cemented sand from this experimental study and data from existing literature is presented. The data with axial strain, volumetric strain, and deviatoric stress are digitized from Rad and Clough (1982); Abdulla and Kiousis (1997); Schnaid et al. (2001); Wang and Leung (2008); Marri et al. (2010); Porcino et al. (2012). The digitized values were interpolated to obtain the deviatoric stress (q) and volumetric strain (ε_v) at finite constant increments of axial strain (ε_a); stress-dilatancy behavior was obtained from these variables. For the calculation of dilatancy ($D = \frac{d\varepsilon_v}{d\varepsilon_q}$), slope of the ($\varepsilon_q$ - ε_v) plot is obtained by fitting a line locally to a set of points.

In this article, the term "stress-dilatancy" is used for the description of the behavior at each state, while "strength-dilatancy" is used for the state corresponding to the peak stress ratio (η_p) – maximum dilatancy (D_{max}) point associated with data from different experiments. Due to unknown elastic parameters for digitized studies, total dilatancy (D) instead of plastic dilatancy (D_p) is used; this is also common for studies on cemented sand (Coop and Willson, 2003; Dalla Rosa et al., 2008; Consoli et al., 2011; Rios et al., 2014).

4.1. Normalized stress ratio

To remove the effect of sand mineralogy and morphology (due to different parent sand in different studies) on stress-dilatancy response of cemented sand, a normalized stress ratio ($\frac{M-\eta}{\alpha}$) is used where M is the critical state stress ratio and α is the Nova-Wood stress-dilatancy parameter (Nova and Wood, 1979) for sand. The form of stress-dilatancy equation used here is.

$$D = f\left(\frac{M-\eta}{\alpha}, \chi\right) \tag{1}$$

where χ represents other variables which control the dilatancy of cemented sand such as relative density, cement content, cement type, and mean effective stress.

In establishing and quantifying the effects of structure on the compression behavior of soils, Burland (1990) used void index (I_v, a normalized void ratio) to eliminate the effect of soil type and to bring forth effect of structure on one dimensional compression characteristics of soils. This was later modified to be expressed in terms of stress invariants (Baudet and Stallebrass, 2004; Xu and Coop, 2016; Xu et al., 2018) to accommodate more generalized stress paths. Here, the normalized stress-dilatancy plot also highlights the effect of structure due to cementation and removes the effect of intrinsic parameter related to composition of sand. In this normalized plot, the "intrinsic" behavior of the reconstituted or clean sand will plot on a unique line, by definition, which is termed as the "intrinsic stress-dilatancy line".

Nova and Wood stress dilatancy parameters M and α are obtained by fitting $\alpha D + \eta = M$ to stress-dilatancy response of all the sand experiments (0% cementation, different confining pressures and/or relative density) in each study. As the Nova and Wood stress dilatancy response is only applicable for frictional plastic response, the regression is performed post elastic response and before maximum dilatancy (behavior is affected by localization after maximum dilatancy). Table 2 lists parameters M and α for each dataset.

4.2. Stress-dilatancy of cemented sand from experiments

Fig. 3a and Fig. 3b presents dilatancy (D) vs. normalized stress ratio ($\frac{M-\eta}{\alpha}$) for cemented sand and sand. The initial part of the plot represents elastic contractive response followed by linear response for sand and curved response for cemented sand. The linear stress-dilatancy response of sand is independent of the initial mean effective stress, and relative density (Been and Jefferies, 2004). In Fig. 3a, a linear trend ($\frac{M-\eta}{\alpha} + D = 0$) is fitted to intermediate part of stress-dilatancy response to evaluate the critical stress ratio (M) for sand as 1.3. The curved response of cemented sand in Fig. 3b can be explained by an additional requirement of work in breakage of bonds (Cuccovillo and Coop, 1999). The energy necessary to break the bonds is a function of instantaneous bond strength (number of instantaneous bonds present) which degrades during isotropic compression or during shearing of specimen. The stress-dilatancy response of cemented sand converges to a clean sand response at high confining pressures: the inter-particle bonds break down during the isotropic compression phase at high confining pressures.

In addition to the experiments performed in this research program, a detailed analysis of stress-dilatancy behavior is presented from the data extracted from literature (Rad and Clough, 1982; Abdulla and Kiousis, 1997; Schnaid et al., 2001; Wang and Leung, 2008; Marri et al., 2010) to understand the response with varying confining pressure, relative density, and cement content. The details of extracted data are given in Table3. Specifically attempts

Table 2
Nova and Wood stress dilatancy parameters M and α obtained by fitting $\eta + \alpha D = M$ to the all the sand data available for corresponding study.

Experimental study	M	α
Rad and Clough (1982)	1.20	−0.69
Abdulla and Kiousis (1997)	1.29	−0.55
Schnaid et al. (2001)	1.35	−0.64
Wang and Leung (2008)	1.16	−0.95
Marri et al. (2010)	1.28	−0.62
Current study	1.30	−0.95

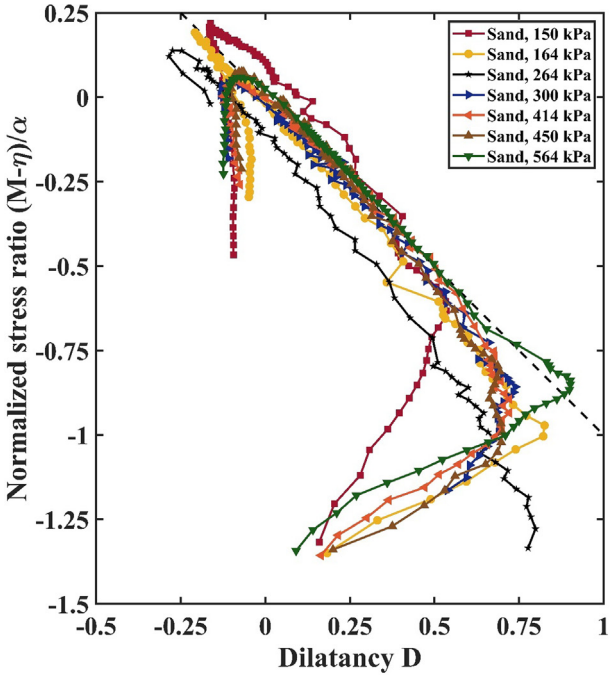

(a) Sand

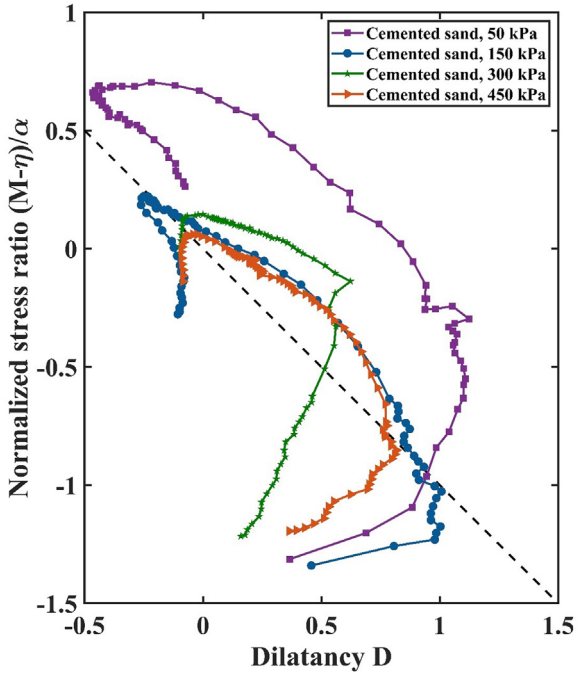

(b) Cemented sand

Fig. 3. Stress-dilatancy behavior of sand and cemented sand.

to highlight the breakage of cohesive bonds which may occur during isotropic compression if the bond strength is less than the confining pressure or otherwise during the shearing process are made. In case of breakage during shearing, a gross yield point can be identified to explain the response.

4.3. Effect of confining pressure

As discussed in the previous paragraphs, with increase in confining pressure the stress-dilatancy plots converge towards a sand response. This behavior can also be observed in Fig. 4 for triaxial experiments performed over a range of confining pressures. The response shown in Fig. 4a corresponds to experiments performed at low confining pressures (Rad and Clough, 1982) on 4% cemented sand prepared at a relative density of 75% (cohesion intercept – 143 kPa, bond strength – 204 kPa). The experiments corresponding to an initial mean effective stress lower than the bond strength show distinct stress-dilatancy response. For specimens consolidated to a stress level above the bond strength, the stress-dilatancy response mirrors that of sand. At very high confining pressures (Marri et al., 2010) as reported in Fig. 4b and Fig. 4c, particle breakage may also play an important role. The experiments shown in Fig. 4b corresponds to 5% cemented sand with cohesion intercept of 1080 kPa and bond strength of 906 kPa. Fig. 4c presents response of 15% cemented sand (cohesion intercept – 7431 and bond strength – 6235 kPa), for confining pressure below the bond strength, stress-dilatancy response is quite distinct whereas at higher confining pressure response tend to become frictional.

4.4. Effect of relative density

The increase in relative density increases the number of contact points between sand particles and consequently, bond strength is higher for high relative density because of the increased propensity of bond formation (Rad and Clough, 1982; Qabany and Soga, 2013). The higher bond density (number of bonds per unit volume of specimen) results in higher stress ratio and in turn will affects the stress-dilatancy response. Fig. 5 shows the effect of relative density (Rad and Clough, 1982) on stress-dilatancy response for different cement content and confining pressure. The maximum stress ratio increases with increase in relative density and cemented sand becomes more dilatant (Fig. 5a). The stress-dilatancy response for 1% and 2% cemented sand tend to collapse on a unique path (Fig. 5b and Fig. 5c) for confining pressure higher than their respective bond strength (Table3).

4.5. Effect of cement content

Fig. 6 shows the effect of cement content on stress-dilatancy response of cemented sand. With increase in cement content, the peak normalized stress ratio and maximum dilatancy increases both at high (Fig. 6a – Marri et al., 2010) and low initial mean effective stress (Fig. 6b – Schnaid et al., 2001). The effect of cement content on the stress-dilatancy response is similar to the effects of relative density. This suggests that at a given confining pressure, a unique stress-dilatancy behavior can be achieved either by increasing cement content (or cement volume)

Table 3
Details of data extracted from literature (CC - cement content, Cp - curing period, ei - initial void ratio, Dr - relative density, c - cohesion intercept, UCS - unconfined compressive strength, Pi'- initial mean effective stress.

Sand & Reference	CC, C_p	Index properties	Method,size (mm)	e_i or D_r	c (kPa), φ_{peak}	UCS (kPa)	$P_i^{'}$ (kPa)
	4%, 14 Days	D_{10}-0.30 mm, D_{50}-0.58 mm, D_{60}-0.67 mm, G_s - 2.65	Tamping procedure D - 70 ± 2 H - 147 ± 1	60%	123, 29°	203	35, 60, 120, 252, 345, 414
				75%	143, 35°	275	35, 120, 252, 414
				90%	153, 41°	350	35, 60, 120, 252, 276, 345
	2%, 14 Days	D_{10}-0.28 mm, D_{50}-0.36 mm, D_{60}-0.40 mm, G_s - 2.65	Constant height drop D - 70 H - 165	25%	12, 34°	25	35, 103, 207
Rounded to subrounded Monterey Sand & Rad and Clough (1982)				50%	20, 36°	42	35, 103, 207, 345
				80%	30, 39°	55	35, 103,207
	1%, 14 Days	D_{10}-0.28 mm, D_{50}-0.36 mm, D_{60}-0.40 mm, G_s - 2.65	Constant height drop D - 70 H - 165	25%	5, 33°	7	35, 103, 207, 345
				50%	9, 35°	2	35, 103, 207, 345
				80%	14, 38°	30	103, 207, 345
	0%, N.A.	D_{10}-0.28 mm, D_{50}-0.36 mm, D_{60}-0.40 mm, G_s - 2.65	Air pluviation	32%	0, 33°	0	103, 207, 345
				45%	0, 35°	0	103, 207, 345
				77%	0, 39°	0	103, 207, 345
Abdulla and Kiousis (1997)	6%, 14 Days	C_u - 2.3, C_c - 0.76, D_{50}- 0.67 mm, G_s - 2.66	Tamping procedure D - 100 H - 100	81%	221, 40°	–	15, 100, 200, 300
	4%, 14 Days			81%	90, 40°	–	15, 100, 200, 300
	2%, 14 Days			48%	35, 40°	–	15, 100, 200, 300
Schnaid et al. (2001)	5%, 7 Days	D_{10}-0.0028 mm, D_{60}-0.09 mm, G_s - 2.70	Tamping procedure D - 50 H - 100	0.51	277, 39°	1168	20, 60, 100
	3%, 7 Days			0.52	138, 44°	737	20, 60, 100
	1%, 7 Days			0.51	57, 41°	305	20, 60, 100
	0%, N.A.		- D - 50 H - 100	0.52	9.9, 35°	0	20, 60, 100
Rounded sand & Wang and Leung (2008)	3%, 7 Days	D_{10}-0.64 mm, D_{50}-0.83 mm, D_{60}-0.90 mm, G_s - 2.65	Tamping procedure D - 70 H -140	0.72	43.9, 32.1°	–	50, 80, 100
	2%, 7 Days			0.72	11.5, 32.1°	–	50, 80, 100
	1%, 7 Days			0.72	7.5, 30.1°	–	50, 80, 100
	0%, N.A.		- D - 70 H - 140	0.72	0.0, 28.6°	–	50, 80, 100
Angular, subangular, and rounded sand & Marri et al. (2010)	15%, 14 Days	D_{10}-0.19 mm, D_{50}-0.40 mm, D_{60}-0.42 mm, G_s - 2.65	Tamping procedure D - 50 H - 100	0.50	7431, 50°	5541	1E3, 4E3, 8E3, 12E3
	10%, 14 Days			0.50	3186, 50°	2213	1E3, 4E3, 8E3, 12E3
	5%, 14 Days			0.50	1080, 50°	564	1E3, 4E3, 8E3, 12E3
	0%, N.A.		Moist tamping D - 50 H - 100	0.50	268, 50°	0	1E3, 4E3, 8E3, 12E3

or increasing relative density (or decreasing the void volume). This provides an explanation for Consoli et al., (2011)'s conclusion that at a given confining pressure and cement-void ratio (ratio of cement volume to void volume), stress-dilatancy relation can be uniquely described for weakly cemented sand. Consoli et al's observation is also validated by Rios et al. (2014). The observation that for initial mean effective stress higher than bond strength results in collapse of cemented sand and sand response (Fig. 6a) also holds well for different cement content (in the regime

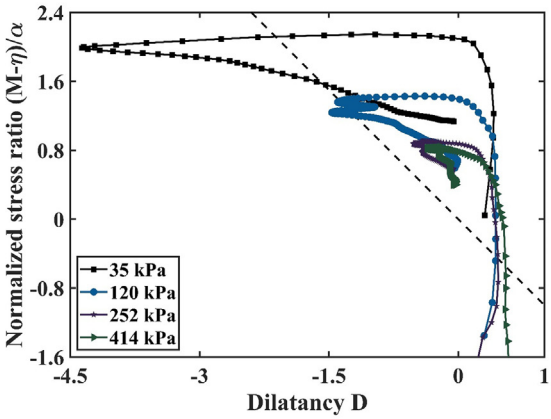

(a) D_R −75%, cement content −4%, Data − Rad and Clough (1982)

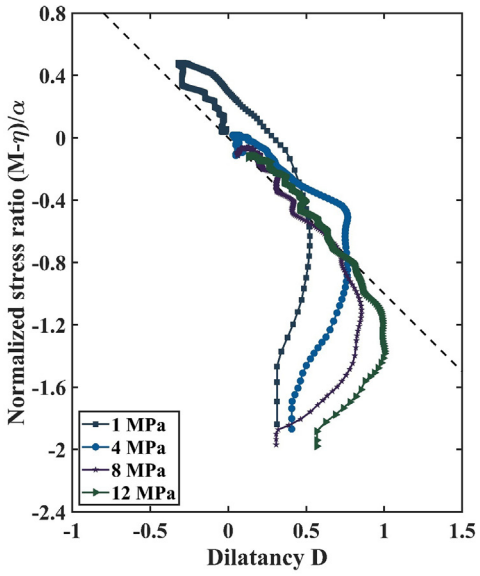

(b) Cement content −5%, Data − Marri et al. (2010)

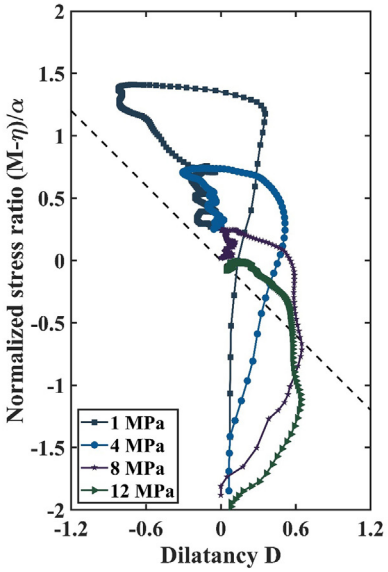

(c) Cement content −15%, Data − Marri et. al (2010)

Fig. 4. Effect of confining pressure on stress-dilatancy behavior.

of weakly cemented sand). This suggests that an important controlling variable in stress-dilatancy response of cemented sand is the ratio of initial cohesion intercept to initial mean effective stress $\frac{c_o}{p_i'}$ (where c_0 captures both the effect of cement content and relative density). Similar results were also obtained from Abdulla and Kiousis (1997) and Wang and Leung (2008).

4.6. Characteristics of stress-dilatancy response for cemented sand

Fig. 7a shows the normalized stress-dilatancy plots corresponding to each study examined in this work. Further, to establish a dependence of stress-dilatancy relation on $\frac{c_o}{p_i'}$, the responses are plotted with varying $\frac{c_o}{p_i'}$ in Fig. 7b. The dash line in these two Figures shows the stress-dilatancy fit for clean sand response (intrinsic stress-dilatancy line). Fig. 7a shows points (black circular markers) corresponding to gross yield of cementation (Coop and Atkinson, 1993; Cuccovillo and Coop, 1999; Coop and Willson, 2003; Alvarado et al., 2012a,b; Gutierrez, 2007). In the elastic domain prior to the gross yield, either a constant dilatancy response with increasing normalized stress ratio or a contractive response is observed. Following the point of yielding, the slope of stress-dilatancy response changes significantly for high values of $\frac{c_o}{p_i'}$, whereas

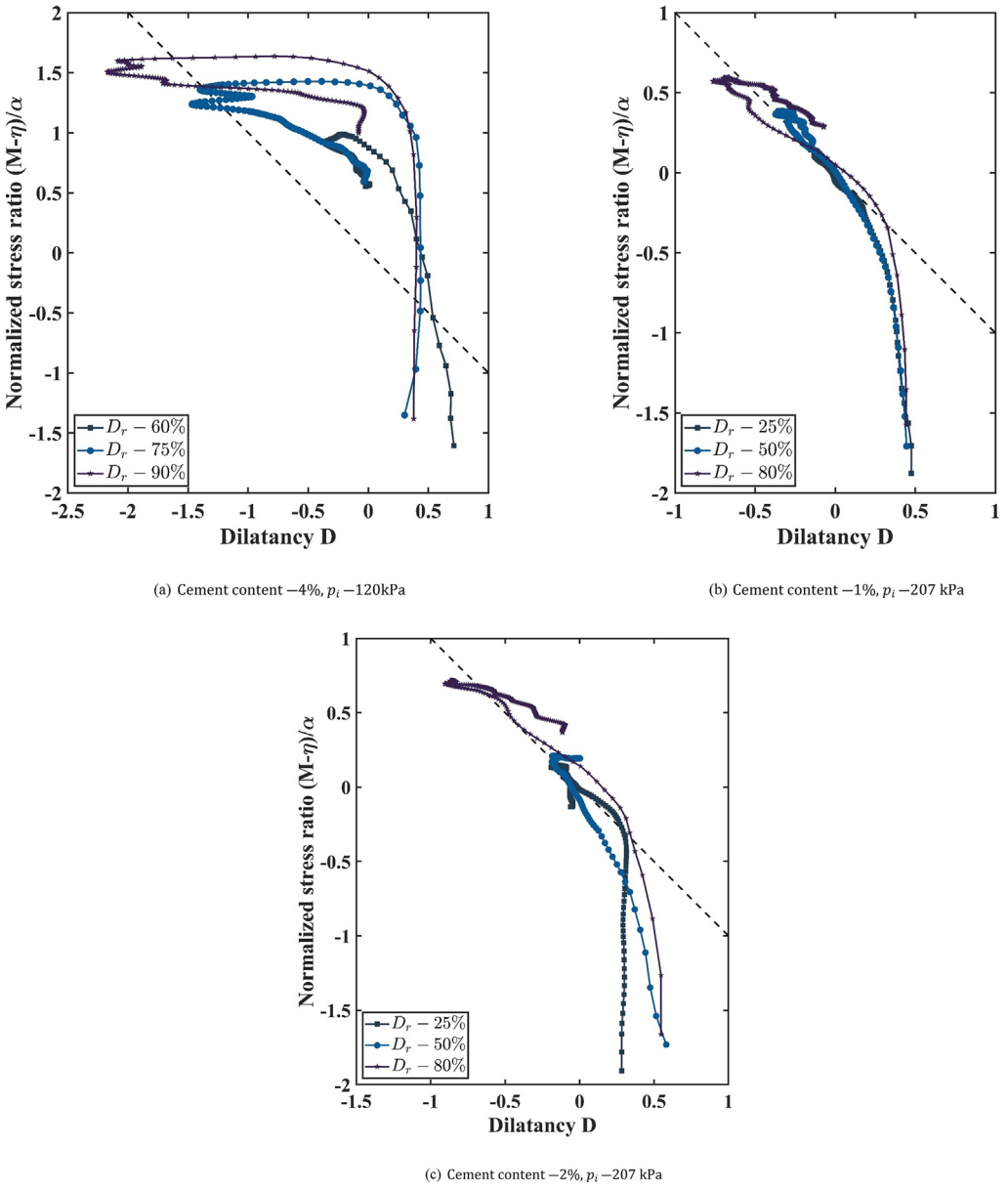

(a) Cement content −4%, p_i −120kPa

(b) Cement content −1%, p_i −207 kPa

(c) Cement content −2%, p_i −207 kPa

Fig. 5. Effect of relative density on stress-dilatancy behavior, Data-Rad and Clough (1982).

for low values of $\frac{c_o}{p_i'}$ the response converges towards sand behavior. The cemented sand reaches a peak stress ratio well before maximum dilatancy i.e., a significant lag is observed which diminishes for low values of $\frac{c_o}{p_i'}$ (detailed in Fig. 8). The stress-dilatancy response of cemented sand shows a clear relation with $\frac{c_o}{p_i'}$, as $\frac{c_o}{p_i'} \to 0$ response is similar to clean sand and with increasing $\frac{c_o}{p_i'}$ the response tends towards a bi-linear behavior (Fig. 7b). The gross yield points are extracted from Fig. 7a or Fig. 7b and the normalized stress ratio at gross yield is plotted with $\frac{c_o}{p_i'}$ in Fig. 7c; and following fit for the locus of gross yielding is obtained.

$$\left.\frac{M-\eta}{\alpha}\right|_{bond \quad yield} = a\,exp\left(-b\frac{c_o}{p_i'}\right) + c \tag{2}$$

where a = −3.0, b = 0.33, c = 2.32 are constants.

The experimental data points suggest that the normalized stress ratio at yield tends to saturate with increasing $\frac{c_o}{p_i'}$.

4.7. Locus of peak stress-ratio and maximum dilatancy

Fig. 8 presents normalized stress ratio vs. dilatancy plots with locus of peak stress ratio and maximum dilatancy for different experimental studies. At high cement content, the locus of peak stress ratio does not converge to the locus of maximum dilatancy. However, with low cement content, the two loci tend to coincide and for clean sand the two loci merge. This is observed for all the data used in this study (Fig. 8).

The two divergent loci (for peak stress ratio and maximum dilatancy) for cemented sand suggest that a

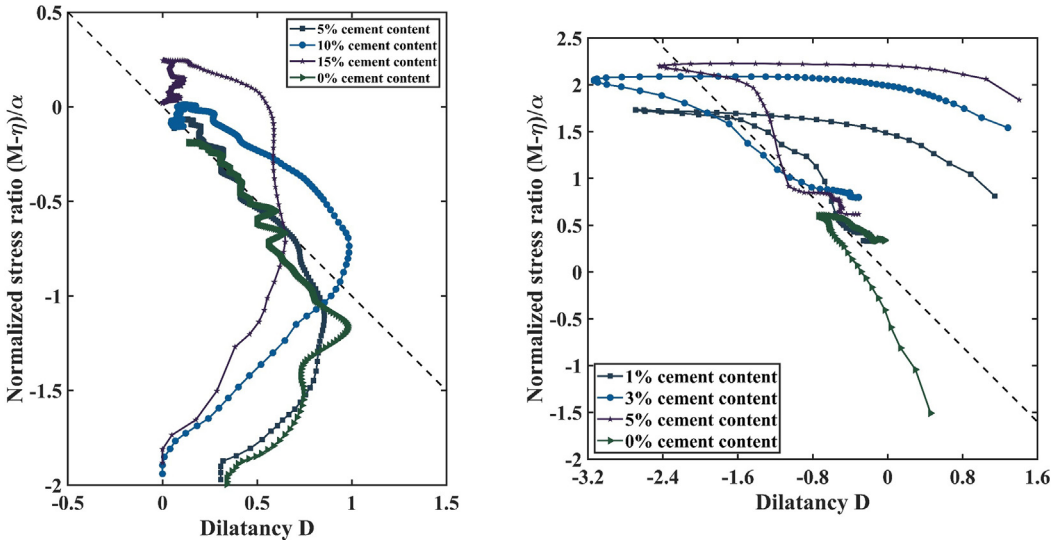

Fig. 6. Effect of cement content on stress-dilatancy behavior.

strength-dilatancy relation, similar to sand, cannot be used in the context of cemented sand.

4.8. Stress-dilatancy relations for cemented sand

In this section, a summary of Rowe's (Rowe, 1962) and Zhang-Salgado (Zhang and Salgado, 2010) stress-dilatancy relations is provided. These relations are further explored to simulate stress-dilatancy behaviour of cemented sand.

Rowe's stress-dilatancy relation (Rowe, 1962) has been source of sand constitutive models (Wan and Guo, 1998; Yu, 1998). The formulation of Rowe's stress-dilatancy relation uses the minimum energy principle along with equilibrium consideration for granular systems. The Eq. (3) presents the Rowe's stress-dilatancy relation.

$$D = \frac{9(M-\eta)+3R_c}{9+(3-2\eta)M+2R_c}$$

$$R_c = \frac{2c(3-M)}{p'}\sqrt{\frac{2M+3}{3-M}} \tag{3}$$

The assumption of applicability of minimum energy principle for a frictional dissipative system was criticized by de Jong (1976). de Jong proposed an alternative approach based on the friction laws and equilibrium considerations which resulted in same relation (Eq. (3)) as of Rowe's for sand.

Zhang and Salgado (2010) observed that for cemented granular system, following the de Jong's approach and using stress transformation, the form of stress-dilatancy relation (Eq. (4)) does not remain same to Rowe's (Eq. (3)).

$$D = \frac{9(M-\eta)-3m_c}{9+(3-2\eta)M+m_c}$$

$$m_c = \frac{6(3-M)}{(3-\eta)}\left(\frac{c}{p'}\right)^2 + \frac{2c(3-M)}{p'} \times \sqrt{\left(\frac{\frac{3c}{p'}}{3-\eta}\right)^2 + \frac{2\eta+3}{3-\eta}} \tag{4}$$

Refer to Appendix B and Appendix C for conversion of stress-dilatancy equation from rendulic or triaxial plane to D vs. η form. A comparison of performance of these stress-dilatancy equations is given in the Fig. 9 for cemented sand ($M = 1.0$, stress path $\frac{\delta q}{\delta p} = 3$). Zhang-Salgado's stress dilatancy relation shows more contractive response before zero dilatancy point and more dilative response later in comparison to Rowe's stress-dilatancy relation. The difference between two relations increases with increase in c/p'_i.

4.9. Key points

The main observations on the mechanical response of cemented sand are presented below as obtained in this study. These observations form a basis for modification in existing stress-dilatancy relation.

- Stress transformation for weakly cemented sand only works for low strain range (until bond yield). For larger strains, stress transformation should be accompanied by the cementation degradation.
- Stress-dilatancy plots of triaxial compression test for uncemented sand collapse along a unique line i.e. intrinsic stress-dilatancy line, whereas the point of peak stress ratio or minimum dilatancy changes with relative density and confining pressure. For cemented sand, it is observed that
  - o For p'_i less than c_0, stress-dilatancy response varies with confining pressure, cement content, relative density.

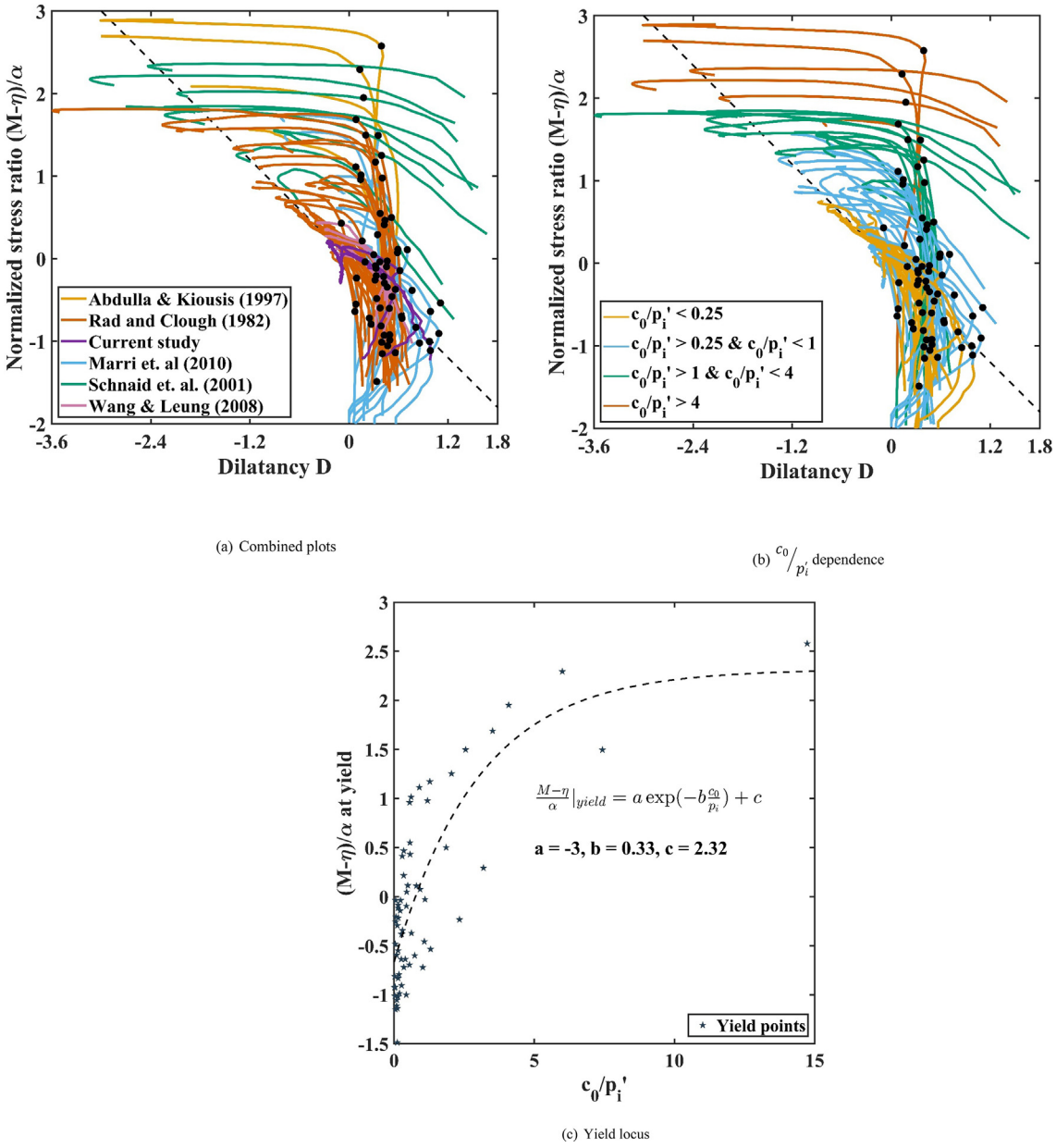

(a) Combined plots

(b) c_0/p_i' dependence

(c) Yield locus

Fig. 7. Normalized stress ratio vs. dilatancy (black circular markers corresponds to gross yield) and gross yield locus.

- If the p'_i is higher than c_0, stress-dilatancy responses converge to sand response.
- Further increase in p'_i results in a behavior similar to sand.

- The stress-dilatancy plot for pure sand is often linear (Been and Jefferies, 2004) i.e., a linear stress-dilatancy behavior might also suggest a purely frictional interaction. For cemented sand, if the bond strength is significantly higher than initial mean effective stress, shearing results in a linear or bi-linear stress-dilatancy plot, whereas if the bond strength is in the range of initial mean effective stress, stress-dilatancy plot is predominantly curved except for the post peak behavior which appears to be linear in most plots discussed here.
- The stress-dilatancy response for cemented sand shows a lower dependence on the initial density than the initial mean effective stress.
- The use of normalized stress ratio facilitates the comparison of effect of cementation between different cemented sand by removing the component of sand composition.
- The normalized stress ratio corresponding to gross yielding of cementation increases with increasing $\frac{c_0}{p_i'}$ and goes towards a constant value as $\frac{c_0}{p_i'} \rightarrow \infty$.
- A strength-dilatancy relation cannot be used for cemented sand since occurrence of maximum dilatancy does not correspond to the occurrence of peak stress ratio.

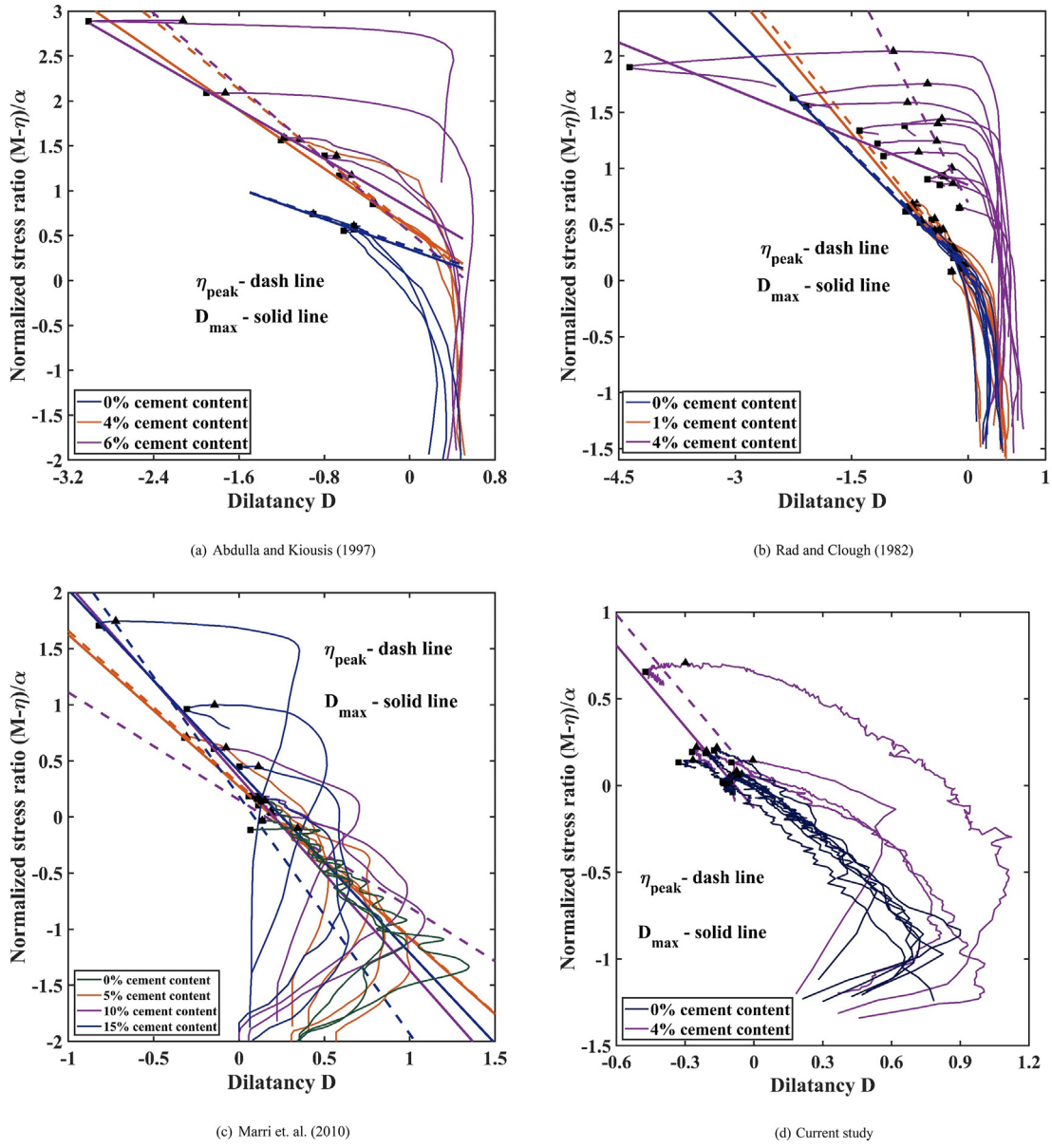

Fig. 8. Locus of peak stress ratio and minimum dilatancy points from extracted data and current study.

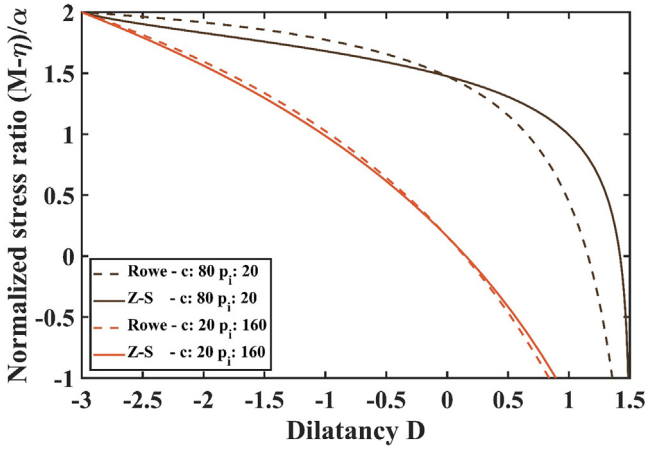

Fig. 9. Stress-dilatancy relations for cemented sand and equivalent sand.

- Rowe's or Zhang-Salgado's stress-dilatancy response, for cemented sand, shows a similar trend as obtained in experiments for increasing $\frac{c_o}{p_i'}$ (Appendix D) where cohesion intercept is a function of cement content, type of cement, curing period, and relative density.

While it is observed that the Rowe's and the Zhang-Salgado's stress-dilatancy relations can be used for first order estimate of the response, the predictions are not satisfactory, due to the assumption of persisting cohesion or cementation through the shearing process.

4.10. Prediction of stress-dilatancy behavior

To predict the stress-dilatancy response, the elastic region (before yielding of bonds) is demarcated from

plastic region (after yielding of bonds) with yield locus as discussed in the ensuing.

4.11. Volumetric response before gross yield

Cemented sands show a constant ratio of incremental volumetric strain to incremental deviatoric strain before gross yield (Fig. 7a). This behaviour can be explained using theory of elasticity:

For an isotropic elastic solid

$$dp = Kd\varepsilon_v^e \tag{5}$$

$$dq = 3Gd\varepsilon_q^e \tag{6}$$

where K, G are bulk and shear modulus respectively. $d\varepsilon_v^e$ and $d\varepsilon_q^e$ are the incremental elastic volumetric and effective deviatoric strains.

For a triaxial compression stress path ($q = 3\ (p\text{-}p_i)$)

$$\frac{dq}{dp} = 3 \tag{7}$$

From Eq. (5), Eq. (6), and Eq. (7)

$$Gd\varepsilon_q^e = Kd\varepsilon_v^e \tag{8}$$

$$D^e = \frac{G}{K} \tag{9}$$

$$D^e = \frac{1-2v}{2(1+v)} \tag{10}$$

where D^e is the ratio of incremental elastic volumetric strain to increment elastic deviatoric strain, nu is the Poisson's ratio.

Before the gross yield, D^e remains constant as eta increases for a linear elastic isotropic solid.

4.12. Stress-dilatancy – post yield

As discussed in previous section, the post yield behavior is primarily characterized by degradation of cementation. For an accurate prediction, a precise model with bond degradation would require more exploration of physics of damage of bonds with different boundary conditions. For simplicity, cohesion softening (Eq. (11)) is introduced based on the idea that the rate of degradation is inversely proportional to the instantaneous bond strength and the inter-particle bonds (participating in shearing process) are completely broken down before the specimen reaches a peak strength i.e. $c(\eta > \eta_p) = 0$ (or for $\eta > \eta(D_{max})$ which are nearly equal). This assumption is supported by experimental and numerical studies (Coop and Willson, 2003; Wang and Leung, 2008) which suggest that post peak response is frictional. The gross yield curve (Fig. 7c) is used to demarcate the elastic and plastic region i.e., c_o remains constant till $\eta \leq \eta_{yield}$. The following relation is derived based on the above assumptions -

$$\begin{aligned} c &= c_o \quad at\ \ \eta = \eta_{yield} \\ c &= c_o\sqrt{\frac{\eta_p - \eta}{\eta_p - \eta_{yield}}} \quad for \quad \eta_{yield} \leq \eta \leq \eta_p \\ c &= 0 \ \ for\ \eta > \eta_p \end{aligned} \tag{11}$$

where c_o is the initial bond strength, η_{yield} is the stress ratio at which gross yielding commences - estimated using Eq. (2) and η_p is the peak stress ratio. The parameters, c_o and η_p (65 and 1.19, Fig. A1) can be determined experimentally along with critical stress ratio M (1.30, Fig. 3a and Table2). Although, it is established in the previous sections that initial bond strength is a function of relative density, cement

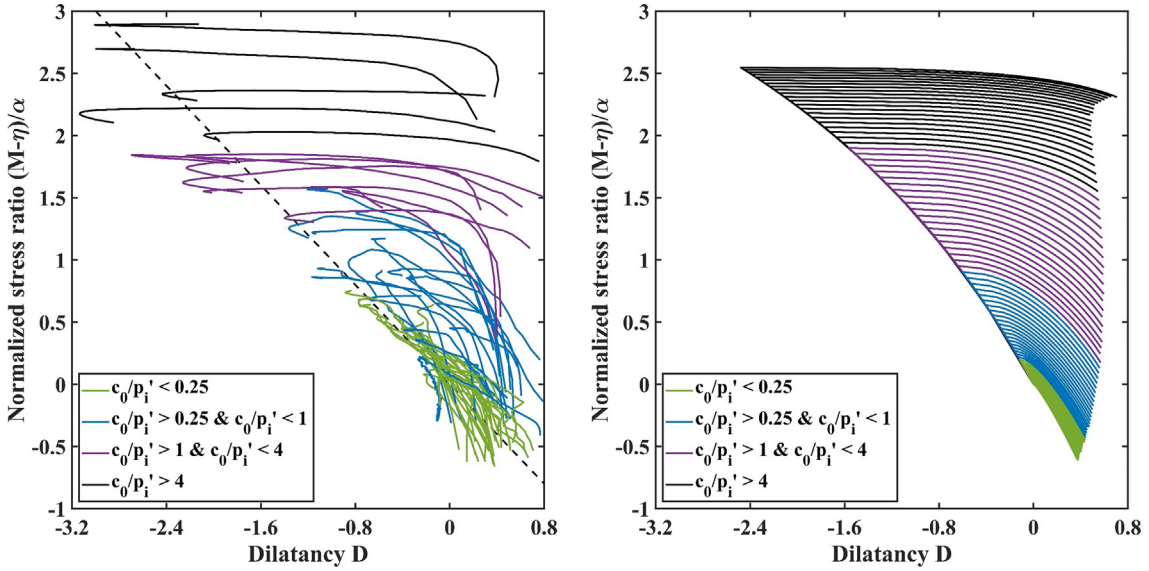

Fig. 10. Performance of stress-dilatancy relations post yield points.

content (also type of cement and curing period), and initial mean effective stress but due to lack of experimental data, a constant c_o is assumed at the end of isotropic compression. A relation of c_o with *Dr*, p_i', *CC*, if known, can readily be incorporated into Eq. (11).

This simple degradation effect (Eq. (11)) is incorporated into Rowe's stress-dilatancy relation. Fig. 10 shows the prediction of post yield stress-dilatancy behavior for varying values of $\frac{c_o}{p_i'}$; Fig. 10a shows the experimental stress-dilatancy response post-yield and Fig. 10b shows corresponding predictions. It is quite apparent that at small values of $\frac{c_o}{p_i'}$ the predictions are very good while at very large values, experimental results show excessive dilation which crosses the dilatancy bounds of Rowe's stress-dilatancy relation (Appendix D).

5. Conclusions

The stress-dilatancy response of cemented sand is studied from the experiments carried out in this study and from the data published in the literature; effect of cement content, confining pressure, and relative density is discussed. The parent sand in these studies were different, and a direct comparison of stress-dilatancy responses was not viable: a normalized stress ratio $\frac{M-\eta}{\alpha}$ is proposed to bring out similarities and facilitate the comparison in stress-dilatancy responses. The responses are found to be a function of $\frac{c_o}{p_i'}$ where c_o is the cohesion intercept which accounts for the effect of cement type, cement content, curing period, and relative density. The characteristics of stress-dilatancy response are discussed with respect to occurrence of yield points, points of peak stress ratio, and points of maximum dilatancy.

The currently available suite of stress-dilatancy relations is examined for cemented sand. It is concluded that the Rowe's or Zhang-Salgado's stress-dilatancy relations are most suitable for cemented sand although not in their original form which assumes persistence nature of cohesion. A gross yield curve is identified and used to delineate the elastic domain of stress-dilatancy response to plastic domain. The gross yield curve provides the stress ratio at yield for different values of $\frac{c_o}{p_i'}$, the degradation of cohesion is introduced after stress ratio reaches its yield value. A simple cohesion degradation model is introduced that improves the prediction of stress-dilatancy response.

Acknowledgements

Authors wish to thank Prof. Beatrice Baudet for her suggestions which resulted in improved manuscript. Authors would also like to acknowledge SERB, Department of Science and Technology, India funding to carry out the experiments.

Appendix A. Cohesion intercept and bond strength

Fig. A1 presents the peak stress state, the locus of the peak stress state has an intercept of 135.6 kPa on *q*-axis with peak stress ratio of 1.19 and the evaluated bond strength (defined as tensile strength or intercept on *p'* axis - Gao and Zhao (2012)), and cohesion intercept (*c*) are 114 kPa and 65 kPa, respectively. The cohesion intercept for control sand is 0 and peak stress ratio is 1.37.

Appendix B. Rowe's stress-dilatancy relation

The original form of Rowe's (Rowe, 1962) stress-dilatancy relation for a stress path lying on the rendulic plane or triaxial plane (Rowe, 1962)

$$\frac{\sigma_1}{\sigma_3} = tan^2\left(\frac{\pi}{4}+\frac{\phi}{2}\right)\left(1-\frac{\dot{\varepsilon}_v}{\dot{\varepsilon}_1}\right) + \frac{2c}{\sigma_3}tan\left(\frac{\pi}{4}+\frac{\phi}{2}\right)\left(1-\frac{\dot{\varepsilon}_v}{\dot{\varepsilon}_1}\right) \tag{B1}$$

To convert this equation into a three-dimensional stress-dilatancy relation, assuming independence from lode angle, σ_1 and σ_3 are substituted in terms of *q* and *p*. Where q = σ_1 - σ_3 and $p = \frac{\sigma_1+2\sigma_3}{3}$. Also, $\sigma_1 = \frac{3p+2q}{3}$, $\sigma_3 = \frac{3p-q}{3}$,

$$\frac{\sigma_1}{\sigma_3} = \frac{3p+2q}{3p-q} = \frac{3+2\eta}{3-\eta} \tag{B2}$$

where η is the stress ratio, ratio of *q* to *p*. Similarly, $\dot{\varepsilon}_1$ is written in terms of $\dot{\varepsilon}_v$ and $\dot{\varepsilon}_q$ with $\dot{\varepsilon}_q = \frac{2}{3}(\dot{\varepsilon}_1 - \dot{\varepsilon}_3)$.

$$\dot{\varepsilon}_1 = \frac{\dot{\varepsilon}_v + 3\dot{\varepsilon}_q}{3} = \dot{\varepsilon}_q\left(\frac{D+3}{3}\right) \tag{B3}$$

where *D* is the dilatancy, ratio of $\dot{\varepsilon}_v$ to $\dot{\varepsilon}_q$. Now, a relation between $tan^2\left(\frac{\pi}{4}+\frac{\phi}{2}\right)$ and crtical state stress ratio $M\left(\frac{q_{CS}}{p_{CS}}\right)$ is established. As specimen reaches critical state, cohesion

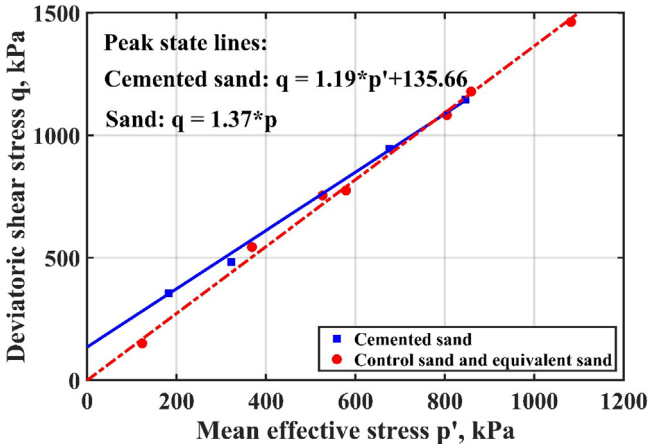

Fig. A1. Peak stress state plot for cemented sand, control sand, and equivalent sand for initial density of 15 kN/m^3. Intercept on p'-axis, bond strength-114 kPa.

will be completely destroyed and $\sigma_1^{cs} = \sigma_3^{cs} tan^2\left(\frac{\pi}{4}+\frac{\phi}{2}\right)$ i.e. $tan^2\left(\frac{\pi}{4}+\frac{\phi}{2}\right) = \frac{\sigma_1^{cs}}{\sigma_3^{cs}}$. From Eq. (B2),

$$tan^2\left(\frac{\pi}{4}+\frac{\phi}{2}\right) = \frac{3+2M}{3-M} \tag{B4}$$

Substituting these into Eq. (B1),

$$\left(\frac{3+2\eta}{3-\eta}\right) = \left(\frac{3+2M}{3-M}\right)\left(\frac{3-2D}{3+D}\right) + \frac{6c}{(3-\eta)p} \times \sqrt{\frac{3+2M}{3-M}\frac{3-2D}{3+D}} \tag{B5}$$

on simplifying,

$$D = \frac{9(M-\eta)+3R_c}{9+(3-2\eta)M+2R_c} \tag{B6}$$

$$R_c = \frac{2c(3-M)}{p'}\sqrt{\frac{2M+3}{3-M}} \tag{B7}$$

Appendix C. Zhang-Salgado's stress-dilatancy relation

The form of Zhang and Salgado's (Zhang and Salgado, 2010) stress-dilatancy relation is,

$$\frac{\sigma_1}{\sigma_3} = tan^2\left(\frac{\pi}{4}+\frac{\phi}{2}\right)\left(1-\frac{\dot{\varepsilon}_v}{\dot{\varepsilon}_1}\right) + \frac{2c}{\sigma_3}tan\left(\frac{\pi}{4}+\frac{\phi}{2}\right)\sqrt{\left(1-\frac{\dot{\varepsilon}_v}{\dot{\varepsilon}_1}\right)} \tag{C1}$$

using a similar procedure as above, following can be derived.

$$D = \frac{9(M-\eta)+3m_c}{9+(3-2\eta)M+m_c} \tag{C2}$$

$$m_c = \frac{6(3-M)}{3-\eta}\left(\frac{c}{p'}\right)^2 + \frac{2c(3-M)}{p'} \times \sqrt{\left(\frac{\frac{3c}{p'}}{3-\eta}\right)^2 + \frac{2\eta+3}{3-\eta}} \tag{C3}$$

Appendix D. Effect of confining pressure and cement content on Rowe's and Zhang-Salgado's relation

Fig. D1 shows the variation of Rowe's stress-dilatancy response with changing $\frac{c}{p_i'}$. With increase in cohesion intercept, the cemented response diverges from sand whereas with increase in initial mean effective stress, the cemented sand response converges towards sand response. For a very high value of c or a very low value of p_i' such that $\frac{c}{p_i'} \to \infty$ dilatancy tends towards 1.5. As specimen is further sheared in triaxial compression p' increases and $R_c \to 0$. Also note that for triaxial compression $\eta = 3\left(1-\frac{p_i'}{p'}\right)$, with increasing p', $\eta \to 3$. For $R_c \to 0$ and $\eta \to 3$, D tends to -3. So, for

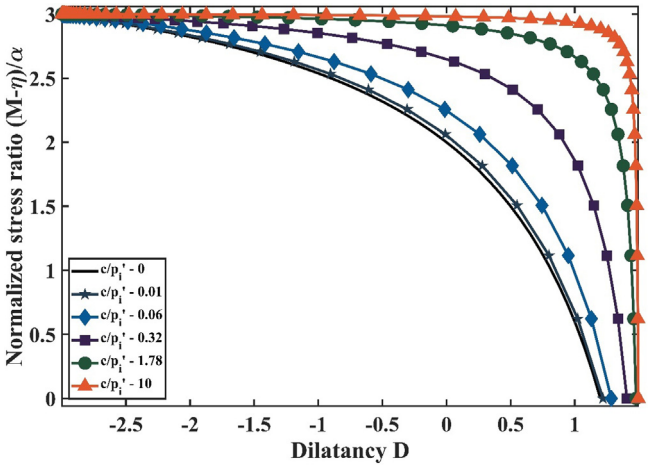

Fig. D1. Rowe's stress-dilatancy relation with initial mean effective stress and cement content.

triaxial compression test on cemented sand, Rowe's relation predicts bounds $D \leq 1.5$ and $D \geq -3$ and $\eta \leq 3$. All the results (except a few, Fig. 7a) present in this study follows these bounds.

A very similar response was obtained from Zhang-Salgado's relation.

References

Abdulla, A.A., Kiousis, P.D., 1997. Behavior of cemented sands|i. testing. Int. J. Numer. Anal. Meth. Geomech. 21, 533–547. https://doi.org/10.1002/(SICI)1096-9853(199708)21:8<533::AID-NAG889>3.0.CO;2-0.

Airey, D.W., 1993. Triaxial testing of naturally cemented carbonate soil. J. Geotech. Eng. 119, 1379–1398. https://doi.org/10.1061/(asce)0733-9410(1993)119:9(1379).

Alvarado, G., Coop, M., Willson, S., 2012a. On the role of bond breakagedue to unloading in the behaviour of weak sandstones. Geotechnique 62, 303–316. https://doi.org/10.1680/geot.8.P.017.

Alvarado, G., Lui, N., Coop, M.R., 2012b. Effect of fabric on the behaviourof reservoir sandstones. Can. Geotech. J. 49, 1036–1051. https://doi.org/10.1139/t2012-060.

Bachus, R.C., Clough, G.W., Sitar, N., Rad, N.S., Crosby, J., Kaboli, P., 1981. Behavior of weakly cemented soil slopes under static and seismic loading conditions, Volume II. techreport 52. The John A Blume Earthquake Engineering Center, Stanford University. Department of Civil and Environmental Engineering, Stanford University.

Baudet, B., Stallebrass, S., 2004. A constitutive model for structured clays. Geotechnique 54, 269–278. https://doi.org/10.1680/geot.2004.54.4.269.

Been, K., Jefferies, M., 2004. Stress dilatancy in very loose sand. Can. Geotech. J. 41, 972–989. https://doi.org/10.1139/t04-038.

Burland, J.B., 1990. On the compressibility and shear strength of natural clays. Geotechnique 40, 329–378. https://doi.org/10.1680/geot.1990.40.3.329.

Caquot, A.I., 1934. Equilibre des massifs a frottement interne: stabilite des terres, pulverulentes ou coherentes. Gauthier-Villars.

Consoli, N.C., Foppa, D., Festugato, L., Heineck, K.S., 2007. Key parameters for strength control of artificially cemented soils. J. Geotech. Geoenviron. Eng. 133, 197{205. https://doi.org/10.1061/(asce)1090-0241(2007)133:2(197).

Consoli, N.C., Cruz, R.C., Fonseca, A.V.D., Coop, M.R., 2011. Influence of cement-voids ratio on stress-dilatancy behavior of artificially cemented sand. J. Geotech. Geoenviron. Eng. 138, 100–109. https://doi.org/10.1061/(asce)gt.1943-5606.0000565.

Coop, M.R., Atkinson, J.H., 1993. The mechanics of cemented carbonate sands. Geotechnique 43, 53–67. https://doi.org/10.1680/geot.1993.43.1.53.

Coop, M., Willson, S., 2003. Behavior of hydrocarbon reservoir sands andsandstones. J. Geotech. Geoenviron. Eng. 129, 1010–1019. https://doi.org/10.1061/(asce)1090-0241(2003)129:11(1010).

Cuccovillo, T., Coop, M.R., 1997. Yielding and pre-failure deformation of structured sands. Geotechnique 47, 491–508. https://doi.org/10.1680/geot.1997.47.3.491.

Cuccovillo, T., Coop, M.R., 1999. On the mechanics of structured sands. Geotechnique 49, 741–760. https://doi.org/10.1680/geot.1999.49.6.741.

Dalla Rosa, F., Consoli, N.C., Baudet, B.A., 2008. An experimental investigation of the behaviour of artificially cemented soil cured under stress. Geotechnique 58, 675–679. https://doi.org/10.1680/geot.2008.58.8.675.

Das, B., Yen, S., Dass, R., 1995. Brazilian tensile strength test of lightly cemented sand. Can. Geotech. J. 32, 166–171. https://doi.org/10.1139/t95-013.

de Jong, G.D.J., 1976. Rowe's stress|dilatancy relation based on friction. Geotechnique 26, 527–534. https://doi.org/10.1680/geot.1976.26.3.527.

Gao, Z., Zhao, J., 2012. Constitutive modeling of artificially cemented sand by considering fabric anisotropy. Comput. Geotech. 41, 57–69 http://www.sciencedirect.com/science/article/pii/S0266352X1100173X.

Gutierrez, G.A., 2007. Influence of late cementation on the behaviour of reservoir sands. PhD thesis. Department of Civil and Environmental Engineering, Imperial College London.

Houlsby, G.T., 1986. A general failure criterion for frictional and cohesive materials. Soils Found. 26, 97–101. https://doi.org/10.3208/sandf1972.26.2_97.

Ismail, M.A., Joer, H.A., Sim, W.H., Randolph, M.F., 2002. Effect of cement type on shear behavior of cemented calcareous soil. J. Geotech. Geoenviron. Eng. 128, 520–529. https://doi.org/10.1061/(asce)1090-0241(2002)128:6(520).

Kandasami, R.K., Singh, S., Murthy, T.G., 2021. Experimental investigations of the stress path dependence of weakly cemented sand. J. Geotech. Geoenviron. Eng. 147. https://doi.org/10.1061/(ASCE)GT.1943-5606.0002475, 04021007.613.

Kim, M.K., Lade, P.V., 1984. Modelling rock strength in three dimensions. International Journal of Rock Mechanics and Mining Sciences & Geomechanics Abstracts. Elsevier, pp. 21–33. https://doi.org/10.1016/0148-9062(84)90006-8.

Lade, P.V., 1982. Three-parameter failure criterion for concrete. J .Eng. Mech. Div. 108, 850–863.

Marri, A., Wanatowski, D., Yu, H., 2010. Drained behaviour of cemented sand at high pressures. Proceedings of the 17th Southeast Asian Geotechnical Conference, pp. 17–20. https://doi.org/10.13140/2.1.3826.8163.

Matsuoka, H., Sun, D., 1995. Extension of spatially mobilized plane (SMP) to frictional and cohesive materials and its application to cemented sands. Soils Found. 35, 63–72. https://doi.org/10.3208/sandf.35.4_63.

Nova, R., Wood, D.M., 1979. A constitutive model for sand in triaxial compression. Int. J. Numer. Anal. Meth. Geomech. 3, 255–278. https://doi.org/10.1002/nag.1610030305.

Porcino, D., Marciano, V., Granata, R., 2012. Static and dynamic properties of a lightly cemented silicate-grouted sand. Can. Geotech. J. 49, 1117–1133. https://doi.org/10.1139/t2012-069.

Qabany, A.A., Soga, K., 2013. Effect of chemical treatment used in micp on engineering properties of cemented soils. Geotechnique 63, 331. https://doi.org/10.1680/bcmpge.60531.010.

Rad, N.S., Clough, G.W., 1982. The Influence of Cementation on the Static and Dynamic Behavior of Sands: John A. Blume Earthquake Engineering Center. Technical Report. Report No. 59, Stanford University, California, December 1982.

Rahimi, M., Chan, D., Nouri, A., 2016. Bounding surface constitutive model for cemented sand under monotonic loading. Int. J. Geomech. 16, 04015049. https://doi.org/10.1061/(ASCE)GM.1943-5622.0000534.

Reddy, K.R., Saxena, S.K., 1992. Constitutive modeling of cemented sand. Mech. Mater. 14, 155–178 http://www.sciencedirect.com/science/article/pii/0167663692900123.

Rios, S., Da Fonseca, A.V., Baudet, B.A., 2014. On the shearing behaviour of an artificially cemented soil. Acta Geotech. 9, 215–226.

Rowe, P.W., 1962. The stress-dilatancy relation for static equilibrium of an assembly of particles in contact. Proc. R. Soc. Lond. A 269, 500–527. https://doi.org/10.1098/rspa.1962.0193.

Schnaid, F., Prietto, P.D., Consoli, N.C., 2001. Characterization of cemented sand in triaxial compression. J. Geotech. Geoenviron. Eng. 127, 857–868. https://doi.org/10.1061/(asce)1090-0241(2001)127:10(857).

Tengattini, A., Das, A., Nguyen, G.D., Viggiani, G., Hall, S.A., Einav, I., 2014. A thermomechanical constitutive model for cemented granular materials with quantifiable internal variables. Part I-theory. J. Mech. Phys. Solids 70, 281–296 http://www.sciencedirect.com/science/article/pii/S0022509614001185.

Wan, R.G., Guo, P.J., 1998. A simple constitutive model for granular soils: modified stress-dilatancy approach. Comput. Geotech. 22 (109–696), 133. https://doi.org/10.1016/s0266-352x(98)00004-4.

Wang, Y., Leung, S., 2008. A particulate-scale investigation of cemented sand behavior. Can. Geotech. J. 45, 29–44. https://doi.org/10.1139/t07-070.

Xu, L., Coop, M.R., 2016. Influence of structure on the behavior of a saturated clayey loess. Can. Geotech. J. 53, 1026–1037. https://doi.org/10.1139/cgj-2015-0200.

Xu, L., Coop, M.R., Zhang, M., Wang, G., 2018. The mechanics of a saturated silty loess and implications for landslides. Eng. Geol. 236, 29-42. URL: http://www.sciencedirect.com/science/article/pii/S0013795217302818. special Issue: Loess Engineering Properties and Loess geohazards.

Yao, Y., Lu, D., Zhou, A., Zou, B., 2004. Generalized non-linear strength theory and transformed stress space. Sci. China Ser. E: Technol. Sci. 47, 691–709. https://doi.org/10.1360/04ye0199.

Yu, H.S., 1998. Casm: A unified state parameter model for clay and sand. Int. J. Numer. Anal. Meth. Geomech. 22, 621–653. https://doi.org/10.1002/(sici)1096-9853(199808)22:8<621::aid-nag937>3.3.co;2-#.

Yu, H.S., Tan, S.M., Schnaid, F., 2007. A critical state framework for modelling bonded geomaterials. Geomech. Geoeng. 2, 61–74. https://doi.org/10.1080/17486020601164275.

Zhang, J., Salgado, R., 2010. Stress{dilatancy relation for mohr-coulomb soils following a non-associated flow rule. Geotechnique 60, 223–226. https://doi.org/10.1680/geot.8.T.039.